*quantum beam science*

MDPI

*Article*

# Magnetic Heating Effect for Quarter-Wave Resonator (QWR) Superconducting Cavities

**Heetae Kim [1,*], Sungmin Jeon [2], Yoochul Jung [1] and Juwan Kim [1]**

[1] Rare Isotope Science Project, Institute for Basic Science, Daejeon 34000, Republic of Korea; niceneph@ibs.re.kr (J.K.)
[2] Department of Physics, Kyungpook National University, Daegu 41566, Republic of Korea
* Correspondence: kimht7@ibs.re.kr

**Abstract:** In this paper, the magnetic heating effect of the superconducting quarter-wave resonator (QWR) cavities is investigated, and the Q slopes of the superconducting cavities are measured with an increasing accelerating field. Bardeen–Cooper–Schrieffer (BCS) resistance is calculated for the zero-temperature limit. The vertical test is shown for the performance test of the QWR cavities. The parameters for the QWR cavity are presented. The Q slopes are measured as a function of an accelerating electric field at 4.2 K. The surface resistance of the superconducting cavity increases with an increasing peak magnetic field. The magnetic defects degrade the quality factor. From the magnetic degradation, we determine the magnetic moments of the superconducting cavities. All quarter-wave resonator (QWR) cryomodules are installed in the tunnel, and beam commissioning is performed successfully.

**Keywords:** superconducting cavity; accelerator physics; vertical test; magnetic defects

check for updates

**Citation:** Kim, H.; Jeon, S.; Jung, Y.; Kim, J. Magnetic Heating Effect for Quarter-Wave Resonator (QWR) Superconducting Cavities. *Quantum Beam Sci.* **2023**, *7*, 21. https://doi.org/10.3390/qubs7030021

Academic Editor: Takeshi Ohshima

Received: 21 April 2023
Revised: 15 June 2023
Accepted: 27 June 2023
Published: 3 July 2023

**Copyright:** © 2023 by the authors. Licensee MDPI, Basel, Switzerland. This article is an open access article distributed under the terms and conditions of the Creative Commons Attribution (CC BY) license (https://creativecommons.org/licenses/by/4.0/).

## 1. Introduction

Superconducting cavities are an important component of a heavy ion accelerator. The superconducting cavities are operated at low temperatures, such as 4.2 K and 2 K. The reducing of field emission sites, electric defects sites, and magnetic defects sites as much as possible is important to maintain the high quality factor of the superconducting cavity. The performance of the superconducting cavity, which includes quality factor, Lorentz force detuning (LFD), pressure sensitivity, X-ray emission, and resonance frequency, is tested at operation temperature, which is called the vertical test. A vertical test facility which included a hanging booth, pits, a solid state power amplifier (SSPA), control racks, and a control room was designed and constructed [1,2]. The performance of the superconducting cavities was tested using a vertical test [3,4]. The field emission, which shows electron emission under a local strong electric field [5–7], and the thermionic emission, which shows electron emission under a local high temperature, were investigated [8,9]. The field emission was studied in terms of dimensions, and the unified theory for the field emission and thermionic emission was also studied [10–12]. The field emission sites of the superconducting cavity were investigated [13–15]; moreover, reductions in the outgassing and the RF processing of the pulsed high peak power for the superconducting cavity were used to reduce the field emission in order to achieve a high-quality cavity [16,17]. The RAON accelerator was designed [18], the quarter-wave resonator (QWR) and the half-wave resonator (HWR) cryomodule were developed [19,20], and the half-wave resonator (HWR) cryomodule was tested at 2 K [21,22]. The high-beta cavity for the quarter-wave resonator (QWR) was tested [23]. Both the electric and magnetic field-dependent surface resistances were studied using a superconducting niobium accelerating cavity [24–26]. For superconducting cavities, medium-temperature furnace baking was performed to improve the quality factor [27], and electro-polishing (EP) was conducted to achieve a high gradient [28]. The shape of the QWR cavity was optimized to achieve a high Q factor for

quantum information systems, and the surface impedance of the superconducting cavities was calculated for quantum computing [29,30].

In this research, we demonstrate the vertical test and measure the Q slopes for the quarter-wave resonators (QWRs) as a function of an accelerating electric field. A magnetic effect is shown in a superconducting cavity. The Q factors are shown as a function of the applied peak magnetic field. The magnetic defects cause the Q factor to degrade. The magnetic moments caused by magnetic defects are obtained by fitting the surface resistance data with BCS resistance, in which the band gap is reduced by magnetic defects. Beam commissioning is presented for QWR cryomodules.

## 2. Magnetic Effect in a Superconducting Cavity

The quality factor of a cavity is defined as the ratio of the stored energy in the resonator to the dissipated energy per cycle by damping processes. The quality factor for the cavity is

$$Q_o = \frac{2\pi U}{P_{dis} T} = \frac{\omega U}{P_{dis}} \tag{1}$$

where $Q_o$ is the quality factor of the cavity, $\omega$ is the angular frequency of the cavity, $U$ is the stored energy of the cavity, $T$ is the period of the cycle, and $P_{dis}$ is the dissipated power in the cavity surface, called the RF surface. The RF power is mainly dissipated in the cavity surface, while some RF power leaves through the input power coupler and transmitted pickup coupler. The quality factor for the input power coupler is defined

$$Q_e = \frac{\omega U}{P_{emit}} \tag{2}$$

where $Q_e$ is the quality factor of the emitted or input power coupler and $P_{emit}$ is the emitted power through the input power coupler.

The quality factor of the transmitted power coupler is defined as

$$Q_t = \frac{\omega U}{P_{tran}} \tag{3}$$

where $Q_t$ is the quality factor of the transmitted power coupler and $P_{tran}$ is the transmitted power through the pickup power coupler.

The loaded quality factor is expressed as

$$Q_L = \frac{\omega U}{P_{tot}} \tag{4}$$

where $P_{tot} = P_{dis} + P_{emit} + P_{tran}$ represents the total power losses in the cavity system. Here, $P_{tot}$ is the total power, $P_{dis}$ is the dissipated power in the cavity walls, $P_{emit}$ is the emitted power, and $P_{tran}$ is the transmitted power.

The stored cavity energy decays when the RF power is turned off, according to the differential equation

$$P_{tot} = \frac{\omega U}{Q_L} \tag{5}$$

From Equation (5), the stored energy is expressed as

$$U = U_0 \exp\left(-\frac{\omega t}{Q_L}\right) \tag{6}$$

where $U_0$ represents the initial stored energy. The decay time becomes

$$\tau_L = \frac{Q_L}{\omega} \tag{7}$$

The $Q_L$ comes from the measurement of the decay time. The cavity quality factor of $Q_o$ can be obtained by defining the quality factors of the couplers as

$$\frac{P_{tot}}{\omega U} = \frac{P_{dis} + P_{emit} + P_{tran}}{\omega U} \tag{8}$$

where $P_{tot}$ is the total RF power, $P_{dis}$ is the dissipated RF power in the cavity, $P_{emit}$ is the emitted RF power, and $P_{tran}$ is the transmitted RF power.

From Equation (8), the quality factors are expressed as

$$\frac{1}{Q_L} = \frac{1}{Q_o} + \frac{1}{Q_e} + \frac{1}{Q_t} \tag{9}$$

The quality factors of Equation (9) become

$$Q_o = (1 + \beta_e + \beta_t)Q_L, \tag{10}$$

where $\beta_e = \frac{Q_o}{Q_e}$ and $\beta_t = \frac{Q_o}{Q_t}$.

The $\beta_e$ can be expressed as

$$\beta_e = \frac{\left(\sqrt{P_{fwd}} \pm \sqrt{P_{ref}}\right)^2}{P_{dis}} \tag{11}$$

where $P_{fwd}$ is the forward power, $P_{dis}$ is the dissipated power in the cavity walls, and $P_{ref}$ is the reflected power. The cavity is over-coupled for $\beta_e > 1$ where the upper sign is used, the cavity is under-coupled for $\beta_e < 1$ where the lower sign is used, and the cavity is critically coupled for $\beta_e = 1$.

The $\beta_t$ can be expressed as

$$\beta_t = \frac{P_{tran}}{P_{dis}} \tag{12}$$

where $P_{tran}$ is the transmitted RF power and $P_{dis}$ is the dissipated RF power on the cavity surface.

The quality factors of Equation (10) becomes

$$Q_o = \left(1 + \frac{\left(\sqrt{P_{fwd}} \pm \sqrt{P_{ref}}\right)^2}{P_{fwd} - P_{ref} - P_{tran}} + \frac{P_{tran}}{P_{fwd} - P_{ref} - P_{tran}}\right) Q_L \tag{13}$$

By controlling the variable power coupler, the beta can be set up with the critical coupling of $\beta_e = 1$. The $\beta_t$ is very small value, in which $Q_t$ is much bigger than $Q_o$. The decay time is measured at the critical coupling, and the loaded quality factor can be expressed as

$$Q_L = \frac{w\tau_{3.01\text{dB}}}{\ln 2} \tag{14}$$

where $3.01\text{dB} = 10^{\left(\frac{3.01}{10}\right)} = 2$.

The accelerating field depends on cavity parameters as well. The accelerating electric field can be expressed as

$$E_{acc} = \sqrt{Q_o P_{dis}\left[\frac{(R/Q)}{L_{eff}^2}\right]} \tag{15}$$

where the geometric shunt impedance of $R/Q$ is the shunt impedance divided by $Q_o$, which measures the beam acceleration efficiency per unit-stored energy U at a resonance frequency, and $L_{eff} = \beta\lambda$ is the effective length of the cavity, in which $\lambda = v/c$ is the velocity over the speed of light. The $R/Q$ and $L_{eff}$ are found using the CST-MWS simulation. The geometric shunt impedance, which depends only on the cavity's shape, needs to be maximized

for cavity design. RF dissipation is reduced by maximizing both the geometric shunt impedance of $R/Q$ and the geometry factor of G.

The accelerating electric field of Equation (15) is expressed as

$$E_{acc} = \sqrt{Q_t P_{tran} \left[ \frac{(R/Q)}{L_{eff}^2} \right]} \tag{16}$$

The accelerating electric field of Equation (16) is written as

$$E_{acc} = \kappa \sqrt{Q_t P_{tran}} \tag{17}$$

where $\kappa = \sqrt{\frac{(R/Q)}{L_{eff}^2}}$ is the kappa of the cavity.

The quality factor is also expressed as

$$Q_o = \frac{Q_t P_{tran}}{P_{fwd} - P_{ref} - P_{tran}} \tag{18}$$

where $P_{fwd}$, $P_{ref}$, and $P_{tran}$ represent the forward RF power, the reflected RF power, and the transmitted RF power, respectively.

The quality factor of the cavity becomes [31]

$$Q_o = \frac{2\pi f \mu \int |H(r)|^2 dV}{\int R_{\mathrm{Sur}} |H(S)|^2 dS} \tag{19}$$

where $f$ is the resonance frequency of the cavity, $H$ is the magnetic field, $\mu$ is the magnetic permeability, $V$ is the cavity volume, and $S$ is the cavity surface area.

The cavity quality factor is expressed as [31]

$$Q_o = \frac{G}{R_{\mathrm{Sur}}} \tag{20}$$

The surface resistance of the superconducting cavity can be expressed as

$$R_{\mathrm{Sur}} = R_{\mathrm{Res}} + R_{\mathrm{BCS}} \tag{21}$$

where $R_{\mathrm{Res}}$ is the residual resistance of the superconducting cavity and $R_{\mathrm{BCS}}$ is the BCS resistance of the superconducting cavity. The BCS resistance depends on temperature, and the residual resistance is the leftover resistance at zero temperature.

Magnetic flux is quantized, and the magnetic flux in the superconductor is quantized with the magnetic flux quantum [32,33]. The trapped magnetic flux, which is the multiple of the magnetic flux quantum in Nb superconducting cavity, can be expressed as [32]

$$\Phi = n \frac{h}{2e} \tag{22}$$

where $n$ is the integer number, and h is the Planck constant. The magnetic defect comes from the trapped magnetic flux of Equation (22). The superconducting current surrounds the quantized magnetic flux, in which the core of the vortex corresponds to its normal state.

The action in nature is expressed as $\mathrm{S} = \int L dt = n\hbar$, in which S is the action and L is the Lagrangian. The reduced Planck constant ($\hbar$) of the minimum action corresponds to the origin of quantization, which includes magnetic flux quantum ($h/2e$), conductance quantum ($2e^2/h$), inverse conductance quantum ($h/2e^2$), von Klitzing constant ($h/e^2$), Josephson constant ($2e/h$), photon ($hf$), etc.

The dissipated power in the superconducting cavity walls is the product of the local surface resistance and the local magnetic field squared over all of the RF surface. The average dissipated power for AC dissipation is expressed as

$$P_{dis} = \frac{1}{2}\int R_S |H(S)|^2 dS \tag{23}$$

where $P_{dis}$ is the dissipated power in the superconducting cavity, $R_S$ is the local surface resistance of the superconducting cavity, $H$ is the local magnetic field over the superconducting cavity surface, and $S$ is the surface area of the superconducting cavity. According to Equation (23), the dissipated power increases as the surface resistance and the trapped magnetic field are increased.

The Cooper pairs in a superconductor show zero resistance towards the DC current, while they show some resistance towards the AC current due to finite momentum. When the temperature is less than half of niobium's critical temperature , $T < T_c/2$, the BCS surface resistance is approximated by [34]

$$R_{\mathrm{BCS}} = \frac{Cf^2}{T}\exp\left(-\frac{\Delta}{k_B T}\right) \tag{24}$$

where $T$ is the temperature in Kelvin, C is the material-dependent constant, $\Delta$ is the band gap of the superconducting material, which represents half of the energy required to break a Cooper pair, and $f$ is the resonance frequency of the superconducting cavity.

The BCS resistance is changed by the presence of magnetic defects in the superconducting cavity, which reduces the band gap energy, with $\Delta = \Delta_0 - MB_{peak}$ [35]. From Equation (24), the BCS resistance is expressed as [35]

$$R_{\mathrm{BCS}} = \frac{Cf^2}{T}\exp\left(-\frac{\Delta_0}{k_B T} + \frac{MB_{peak}}{k_B T}\right) \tag{25}$$

where $\Delta_0$ is the initial band gap, $M$ is the magnetic moment of the superconducting cavity, and $B_{peak}$ is the applied peak magnetic field. The surface resistance of Equation (21) can also be expressed as

$$R_{\mathrm{Sur}} = \frac{Cf^2}{T}\exp\left(-\frac{\Delta_0}{k_B T} + \frac{MB_{peak}}{k_B T}\right) + R_{\mathrm{Res}} \tag{26}$$

where $R_{\mathrm{Res}}$ is the residual resistance. Magnetic defects cause magnetic heating, which causes the pair-breaking of the superconducting current density and the increased density of normal-state electrons. The BCS resistance decreases as the temperature decreases from 4.2 K to 2 K. The surface resistance of Equation (26) shows that the residual resistance and the magnetic resistance coming from the magnetic flux remain at zero temperature.

## 3. BCS Resistance in the Zero-Temperature Limit

The surface resistance of the superconducting cavity is reduced to the residual resistance and the flux-trapped resistance at 0 K because the BCS resistance decreases to zero as the temperature is reduced to 0 K. Figure 1 shows the BCS resistance of Nb as a function of temperature for different cavity frequencies. From Equation (24), the BCS resistance for the Nb superconducting cavity decreases to 8.3, 0.17, and 0 nΩ, respectively, as the temperature is reduced to 4.2, 2, and 0 K for 162.5 MHz. The BCS resistance for the Nb superconducting cavity decreases to 2.1, 0.004, and 0 nΩ, respectively, as the temperature is reduced to 4.2, 2, and 0 K for 81.25 MHz. The BCS resistances of Nb for 81.25, 162.5, and 325 MHz at 4.2 K are about 2, 8, and 32 nΩ, respectively. The BCS resistances of Nb for 81.25, 162.5, and 325 MHz at 2 K are below nΩ.

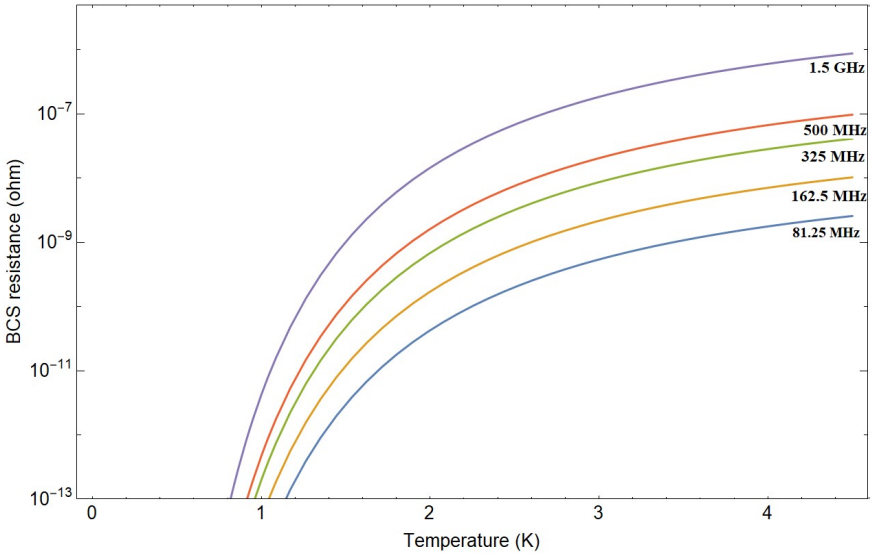



**Figure 1.** BCS resistance of Nb as a function of temperature for different frequencies. The BCS resistance decreases as the temperature decreases. The corresponding frequencies of the BCS resistances, from the bottom to the top, are 81.25 MHz, 162.5 MHz, 325 MHz, 500 MHz, and 1.5 GHz, respectively.

## 4. Experimental Procedures

The residual-resistivity ratio (RRR) 300-grade niobium was used to fabricate superconducting cavities. Figure 2 shows the Nb raw materials. The thickness of the Nb sheet was 3 mm. The dimensions, mechanical properties, and electrical properties of Nb sheet were assessed. The resistivity of Nb was measured as a function of temperature [36]. Young's modulus was measured for mechanical properties.

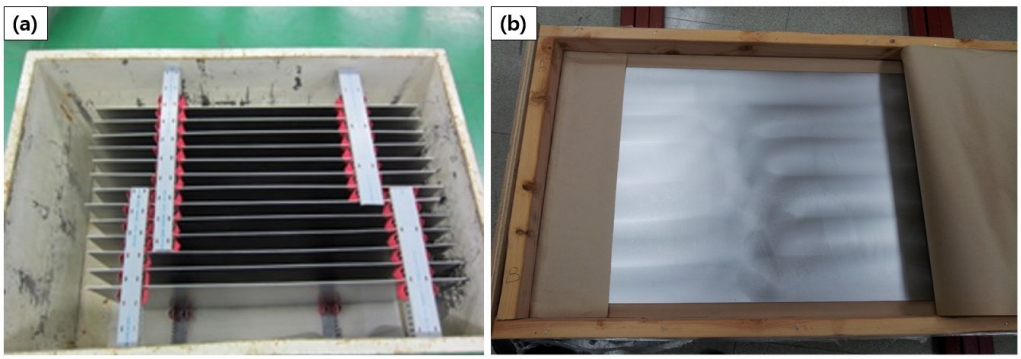



**Figure 2.** Pictures of Nb raw materials: (**a**,**b**) the raw materials of Nb.

The components of the cavity were made using electrical discharge machining (EDM) wire cutting, deep drawing, press forming, and brazing. The resonance frequency of the superconducting cavity was assessed in the stack-up test. The electron beam welding was performed with a vacuum pressure below $5 \times 10^{-6}$ mbar. A visual inspection was performed for the welding beads.

Ultrasonic cleaning was used to clean the cavity surface. First, 1% of liquinox was used at 50 °C for more than half an hour. Second, deionized (DI) water was used at 50 °C for more than half an hour. Buffered chemical polishing (BCP) was performed. The etchant was 49%HF + 69%$HNO_3$ + 85%$H_3PO_4$ (1:1:2 in volume ratio). The etch rate was below 1 µm/min, and the total amount of etching was around 120 µm. The etching temperature was controlled at less than 15 °C because the etching rate increases rapidly as the temperature is increased. The concentration of Nb in the acid solution needs to be less than 15 g/L. The etchant was supplied from the bottom of the quarter-wave resonator (QWR) cavity to the top of the QWR cavity, in which the flow direction was opposite that

of gravity. The etchant came out of the top of the QWR cavity, which is the closed loop circulation. Once the etching was finished, the cavity was turned upside down. Then, deionized (DI) water was supplied to the bottom of the QWR cavity, where it moved from the bottom to the top of the cavity. The deionized (DI) water came out of the top of the QWR cavity, which is also the closed loop circulation.

The inner surface of the cavity was inspected after the buffered chemical polishing (BCP). A uniform and smooth surface is important to prevent a rough surface in the cavity. The rough surface can be a field emission site. High-temperature baking at 600 °C for 10 h was performed in a high-vacuum furnace. The resistivity of deionized (DI) water should be higher than 17 MΩ · cm at 25 °C. High-pressure rinsing (HPR) was used to remove the leftover particles on the cavity surface. The filter size of the high-pressure rinsing was 0.5 μm, and the water pressure was about 100 bars. The diameter of the nozzle was 0.5 mm, and the speed of the nozzle's rotation was around 20 rpm. The total rinsing time for each cavity was over 10 h, of which the rinsing time for each step was over 2 h.

A liquid helium vessel or jacket was attached to the outside of the cavity, and then additional light buffered chemical polishing (BCP) and high-pressure rinsing (HPR) were performed after attaching the jacket. The minimum distance between the outside of the cavity and the jacket was 1 cm, in which liquid helium flows. The dimensions and resonance frequency of the cavity were checked, and then a teak test was performed. To locate the suspected leak sites in the cavity, a helium leak detector was used using a spraying test [37]. The helium leak test was performed at room temperature and then at liquid nitrogen temperature.

The total number of fabricated QWR cavities was 22. Moreover, the performance test for the six QWR cavities was investigated in this research, and the total number of QWR cryomodules was 22.

## 5. Experimental Setup

The RAON accelerator was designed [18]. The quarter-wave resonator (QWR) and the half-wave resonator (HWR) cavity were developed [19,20]. The performance of the QWR cavities was tested at the vertical test facility. Figure 3 shows the schematic diagram for the magnetic shielding in the cryostat. Mu-metal and cryophy were used to reduce the external magnetic field. The X-ray detector is located outside of the cryostat.

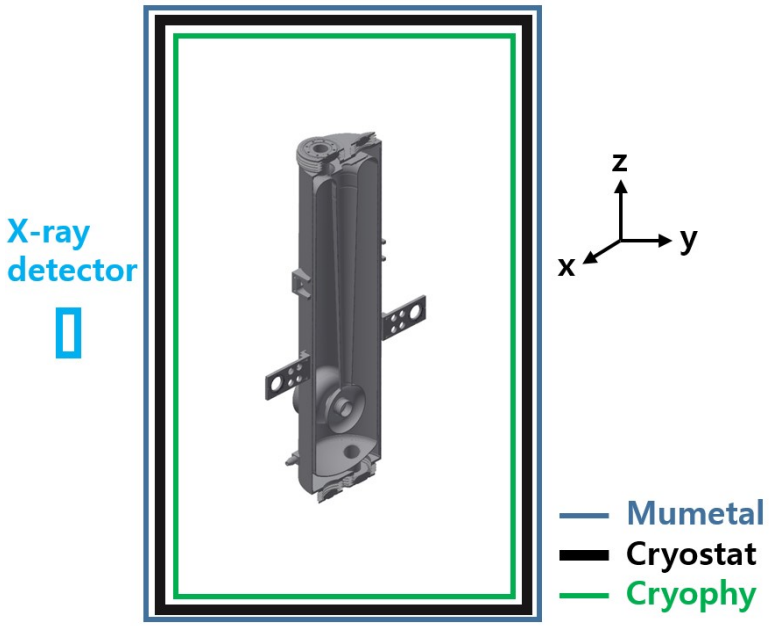



**Figure 3.** Schematic diagram for magnetic shielding in a cryostat. The Mu-metal and cryophy are used to reduce the external magnetic field for the quarter-wave resonator (QWR) cavity test.

Figure 4 shows the cryostat and magnetic shielding. The design of the cryostat, the magnetic shielding, such as the Mu-metal and cryophy, and the top view of the vertical test are shown in Figure 4. Two QWR cavities can be simultaneously tested in the cryostat. The measured static heat load of the cryostat is 8 W. The Mag-03MSB100 Three-Axis Magnetic Field Sensor from Bartington Instruments was used to measure the magnetic field strength. The magnetic field strength for the position of the cavity was below 6 mG after applying the Mu-metal and cryophy.

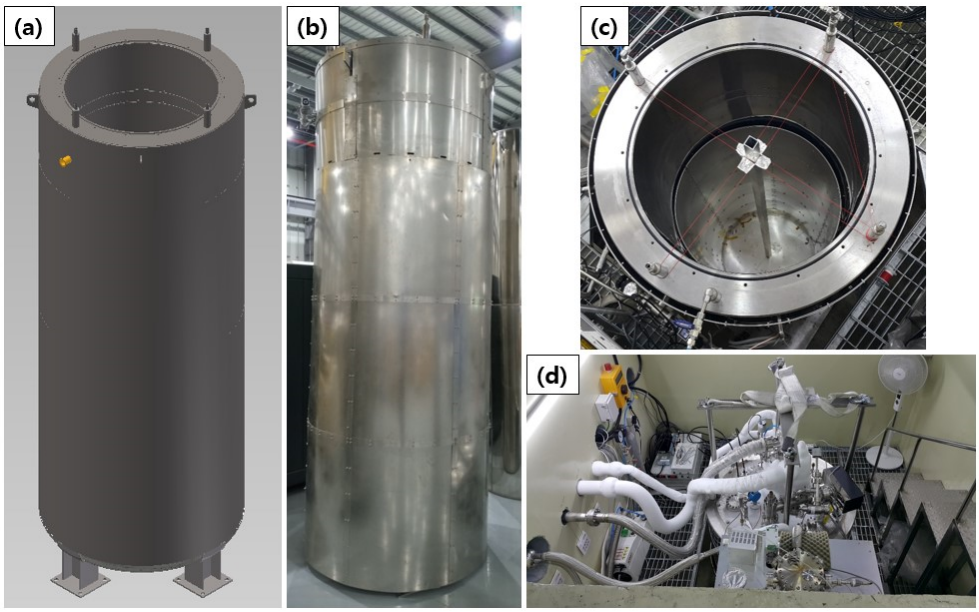



**Figure 4.** Cryostat and magnetic shielding: (**a**) the design of the cryostat, (**b**) the picture of the Mu-metal and cryostat, (**c**) the top view of Mu-metal, cryostat, and cryophy from the outside of the cryostat, and (**d**) the top view of the vertical test.

Table 1 shows the parameters of the quarter-wave resonator (QWR) cavity. The resonance frequency for the QWR cavity is 81.25 MHz. Figure 5 shows the picture of the QWR cavities during vertical test preparation. The temperature sensors, consisting of calibrated Cernox sensors, are attached with kapton tape on the QWR jacket cavities. The physical property measurement system (PPMS) is used to calibrate the Cernox sensors in the temperature range from 1.9 to 325 K [36]. These temperature sensors monitor the temperature of the QWR cavities, while the vapor pressure of the liquid helium shows the temperature of the cavities better because the temperature reading of the sensor depends on how it contacts the cavity and if the liquid helium fills the QWR cavities completely. Two liquid helium level meters were used to monitor the liquid helium level in the cavity and liquid helium vessel.

The QWR cavities were baked at 120 °C for 48 h while a dry pump and a turbo molecular pump (TMP) were used for cavity pumping, which is called the low-temperature baking. The low-temperature baking removes the water from the cavity and is very effective in eliminating multipacting. Low-temperature baking is also necessary to obtain a high Q factor in a high-accelerating electric field.

An X-ray detector was placed outside of the cryostat. The FHZ 632 L-10 gamma detector was used to detect X-ray radiation. Liquid nitrogen and liquid helium were supplied to perform the vertical test, that is, the performance test of the superconducting cavity at 4.2 K. The superconducting cavities were cooled down fast, requiring about an hour, from 150 K to 50 K.

**Table 1.** Parameters for the quarter-wave resonator (QWR) cavity.

| Parameter | QWR |
|---|---|
| Optimum β | 0.047 |
| $f$ [MHz] | 81.25 |
| $L_{eff}(=\beta\lambda)$ [mm] | 173.5 |
| R/Q [Ω] | 469 |
| $E_{peak}/E_{acc}$ | 5.7 |
| $B_{peak}/E_{acc}$ [mT/(MV/m)] | 10.4 |
| $E_{acc}$ [MV/m] | 6.1 |
| $V_{acc}$ [MV] | 1.06 |
| Stored Energy [J] | 4.7 |
| $QR_{Sur}$ [Ω] | 18.1 |

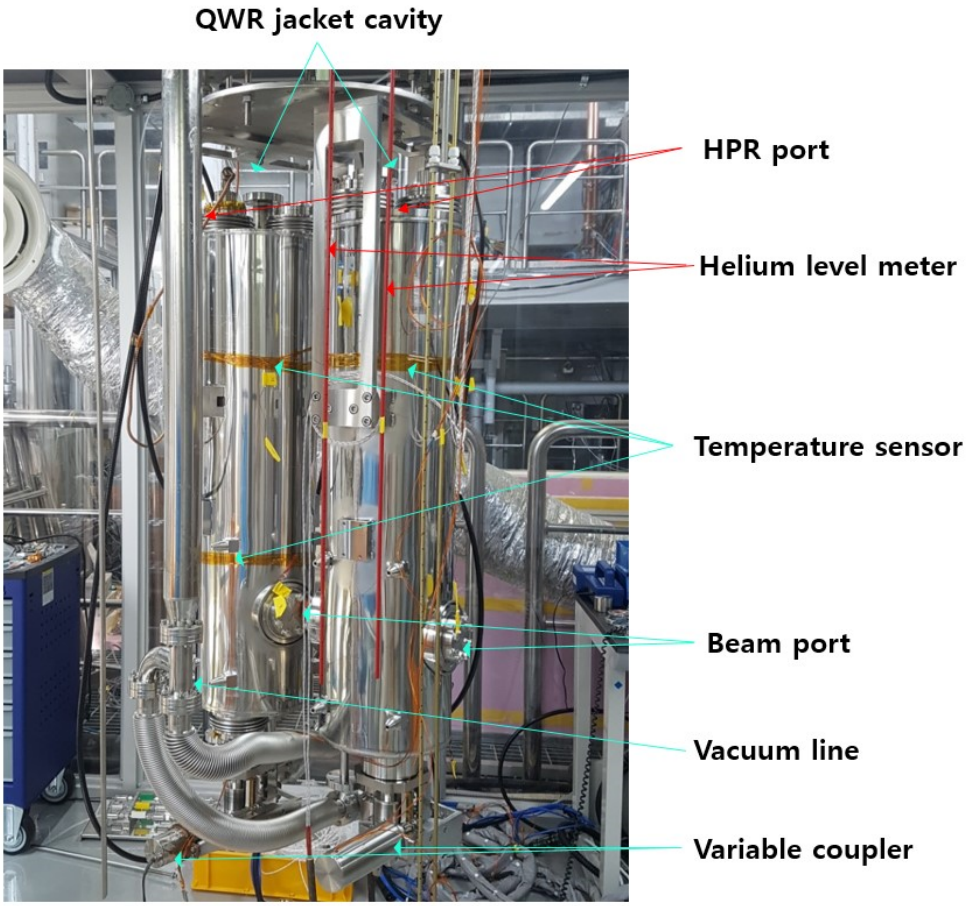



**Figure 5.** A picture of the quarter-wave resonator (QWR) cavities. Two QWR jacket cavities are shown in the hanging booth. The high-pressure rinsing (HPR) ports, liquid helium level meters, temperature sensors, beam ports, vacuum lines, and variable couplers are indicated.

Cable calibration was performed at 4.2 K. Both the forward and reflected power were measured by keeping the input power at 18 dBm. The drive frequency of the Solid State Power Amplifier (SSPA) with 200 W was 81.25 MHz for the QWR cavities. The directional coupler and circulator should work well for 81.25 MHz. S11 and S22 represent the input RF return loss and output RF return loss, respectively. The S21 represents the RF transmission through the cavity. S11, S21, and S22 for each cavity were measured using the Keysight

ENA Network Analyzer E5080A. The bandwidth and loaded Q were measured according to S21, S11, and S22.

RF conditioning can be started at 4.2 K. RF conditioning is a process used to clean the RF surface of the superconducting cavity in order to achieve the highest possible quality factor in the range of all possible accelerating fields. Condensed gases such as water and oxygen on the RF surface of the cavity can be removed using RF conditioning. RF conditioning starts as over-coupled, in which a variable coupler is maximally inserted into the inside of the cavity. The copper antenna of the variable coupler can be moved by about 5 cm. After watching the transmitted power, we changed the forward power and the phase of the low-level radio frequency (LLRF) with self-excited loop (SEL) mode to increase the transmitted power. The forward power and transmitted power increase together after finishing the RF conditioning. It takes about 2 h to 8 h to complete the RF conditioning process for the QWR cavity. The RF power was used from about mW to about 100 W to perform the RF conditioning. The RF power was below 50 W for a high-quality cavity. Pulsed RF conditioning and continuous wave (CW) RF conditioning were used. The pulsed RF conditioning was used for a pulse width of 0.2 s at 1 Hz. The pulsed RF conditioning required more RF power compared to the CW RF conditioning. The reflected RF power decreased to zero when the variable coupler was pulled out to the critical coupling.

The decay time at the critical coupling was measured at 1 MV/m. The decay time for the QWR cavities was about 1 s. X-rays and multipacting should not be generated while the decay time is measured. When there is multipacting, the decay time becomes very short, as in microseconds. The $Q_{ext}$ of the pickup, obtained by using the decay time measurement, was about $10^{11}$.

The Q slope of the QWR cavities was measured from 1 MV/m to the maximum accelerating field, such as 8 MV/m. The quality factor and X-ray radiation are simultaneously measured as functions of the accelerating field. The Q value of the QWR cavities decreases as the accelerating field increases.

## 6. Discussions

The quarter-wave resonator (QWR) is made of Nb, whose phase transition temperature is 9.25 K [36]. The magnetic field trapping coming from the magnetic defects on the RF surface of the superconducting cavity occurs as its temperature decreases and crosses the phase transition temperature of 9.25 K. Therefore, we tried to reduce the external earth magnetic field strength while the QWR cavities were tested.

Figure 6 shows the measurement of the magnetic field strength for the cryostat. The magnetic field strength inside the cryostat is measured from the bottom at a height of 0 cm to the top at a height of 200 cm. The QWR cavity is located between 40 and 140 cm. The Mu-metal is installed outside of the cryostat, the cryophy is installed inside of the cryostat, and the top plate containing the Mu-metal and the cryophy is installed on top of the cryostat. The cryophy is effective at low temperatures, while the Mu-metal is ineffective. The magnetic field strength is measured by installing the Mu-metal, the Mu-metal and cryophy, and the Mu-metal, cryophy, and top plate. The Mu-metal is also installed on the bottom of the cryostat. The magnetic field strength at the location of the QWR cavity decreases to under 6 mG by installing the Mu-metal, the cryophy, and the top plate. The external magnetic field strength causes increased surface resistance of the Nb superconducting cavity due to trapped magnetic flux. The surface resistance is linearly proportional to the external magnetic field strength [38]. In general, the external magnetic field strength for vertical tests is recommended to be below 10 mG. Therefore, 6 mG is sufficient to perform a vertical test.

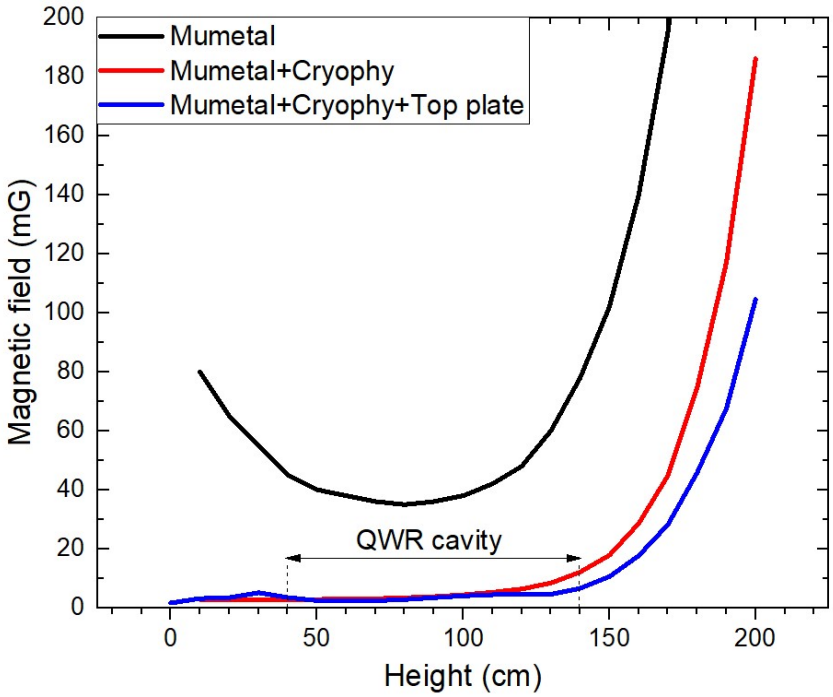



**Figure 6.** Measurement of the magnetic field strength for the cryostat.

The Q slopes are measured with increasing accelerating electric fields for the quarter-wave resonator (QWR) cavities in Figure 7. The Q factor decreases with increasing accelerating fields. The Q factor decreases more rapidly above the accelerating field in which X-ray radiation appears. The field emission effect on the superconducting cavity was investigated [22]. The local temperature of the field emission site increases due to Joule heating, and the electrons emitted from the field emission are accelerated and generate Bremsstrahlung radiation by consuming the RF energy. Therefore, the quality factor of the superconducting cavity decreases with increasing field emission and X-ray generation.

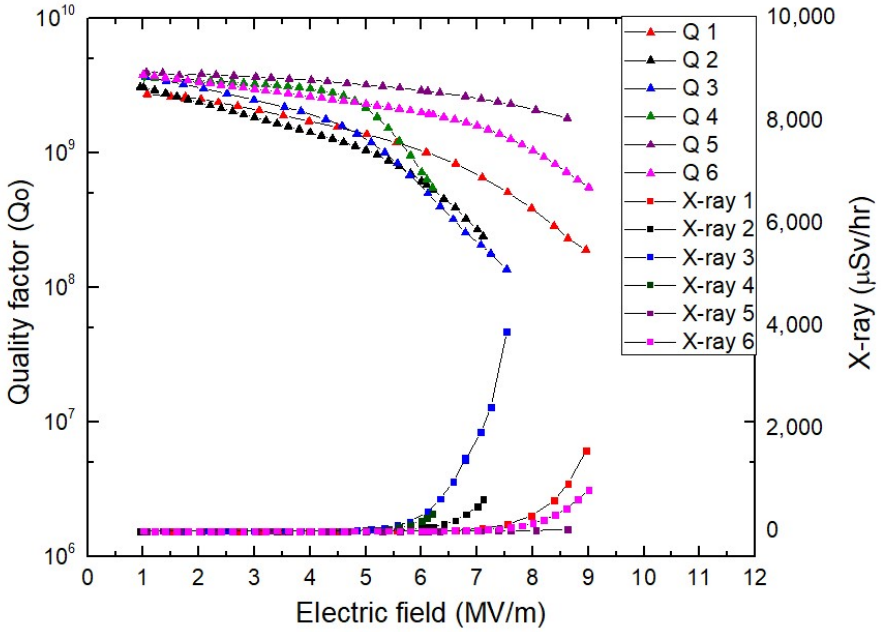



**Figure 7.** Q slope measurement with increasing accelerating fields for the quarter-wave resonator (QWR) cavities. The quality factor of the superconducting cavity decreases with increasing field emission and X-ray generation.

Figure 8 shows the surface resistance measurement as a function of the peak magnetic field strength for the QWR cavities. The surface resistance increases with an increasing peak magnetic field.

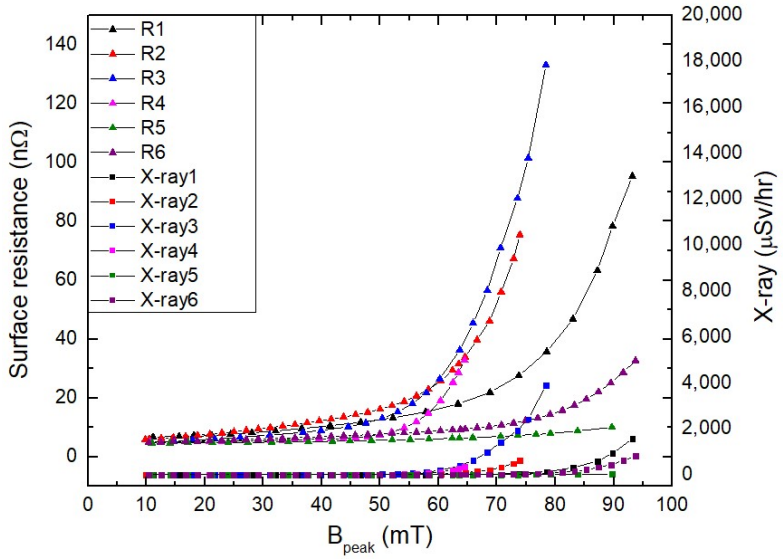



**Figure 8.** Surface resistance measurement as a function of peak magnetic field strength for quarter-wave resonator (QWR) cavities.

The quarter-wave resonator (QWR) cavities are made of niobium, which is a type II superconductor. Type I and type II superconductors are classified by their superconducting coherence length $\xi$ and London magnetic field penetration depth $\lambda$. The superconductor becomes the type I superconductor for $\lambda/\xi < 1/\sqrt{2}$, while the superconductor becomes the type II superconductor for $\lambda/\xi > 1/\sqrt{2}$. The type I superconductors, or soft superconductors, which show zero resistance under DC fields, expel magnetic fields perfectly, which is known as the Meissner effect. The type II superconductors, or hard superconductors, show the Meissner state below the RF critical magnetic field of Hc1, the vortex state, or magnetic flux trapping state, in the range of magnetic field between Hc1 and Hc2, and the normal conducting state in the range of magnetic field above Hc2. According to Equation (23), the dissipated power is proportional to the trapped magnetic field squared. In order to reduce the magnetic heating, it is important to increase the critical magnetic field of Hc1. The niobium material has a residual resistivity ratio (RRR) value of 300 for the QWR cavities. The niobium material has various impurities, which include tantalum, molybdenum, tungsten, titanium, hafnium, zirconium, carbon, nitrogen, oxygen, and hydrogen [39,40]. The critical magnetic field of Hc1 decreases as the defect size increases and the surface roughness increases [41–43]. The oxide layer on the niobium surface works as the magnetic flux pinning sites [44]. Electron-beam welding (EBW) is used to fabricate the QWR cavities. The EBW should be performed in a high-vacuum environment. The EBW was studied to measure the residual-resistivity ratio (RRR) value of Nb as a function of distance from the welding site in terms of the vacuum level, welding power, and welding speed [45]. The defects, such as oxygen, can cause magnetic field trapping while the electron-beam welding (EBW) is performed in a low-vacuum environment. The smooth surface of the E-beam welding sites should be kept; otherwise, the rough surface of the welding site can cause magnetic field trapping.

The surface resistance for the QWR cavities is shown as a function of the peak magnetic field in Figure 9. According to Equation (23), the dissipated power coming from the magnetic heating depends on the surface resistance and magnetic field on the superconducting surface. The magnetic heating causes a decreased quality factor. The surface resistances for the QWR cavities are fitted with the magnetic heating referenced in Equation (26). The magnetic moments for the QWR cavities from 1 to 6 are $3.3 \times 10^{-21}$, $3.4 \times 10^{-21}$, $4.4 \times 10^{-21}$,

$4.3 \times 10^{-21}$, $2.5 \times 10^{-21}$, and $2.3 \times 10^{-21}$ J/T, respectively. The magnetic moments for the QWR cavities are comparable to the magnetic moments of $1.37 \times 10^{-21}$ J/T obtained from the research work [35]. The different magnetic moments obtained in Figure 9 can come from different welding sites, surface roughness, magnetic defects, etc. The magnetic defects of the superconducting QWR cavities cause magnetic heating, which causes the pair-breaking of the superconducting current density and increases the density of normal-state electrons. The magnetic defects causing the trapped magnetic flux can come from welding sites, material defects, surface particles, rough surfaces, etc. In order to fabricate a high-quality superconducting cavity, the magnetic defects should be reduced as much as possible.

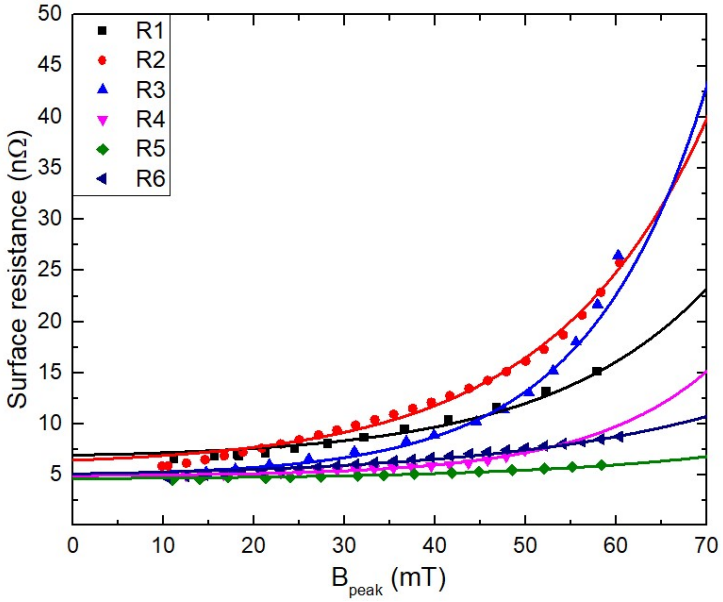



**Figure 9.** Surface resistance as a function of peak magnetic field. According to Equation (23), the dissipated power coming from magnetic heating depends on the surface resistance and magnetic field on the superconducting surface. The surface resistances are fitted with the magnetic heating of Equation (26), and the magnetic moments can be obtained for the cavities.

Degradation of the Q factor results from magnetic heating and X-ray radiation. The Q factor degradation causes increased heating of the superconducting cavity, which requires increased liquid helium evaporation at the operating temperature.

There are 22 QWR cavities in total. The 22 QWR cavities all passed the vertical test, and the QWR cryomodules they were built from passed the horizontal test as well. The quality factor, static heat load, dynamic heat load, pressure sensitivity, Lorentz force detuning (LFD), cavity alignment, X-ray emission, and RF control are measured in the horizontal test. The cavity alignment is within 1 mm in the horizontal test. Following the horizontal test, all of the QWR cryomodules are installed and then cooled down in the RAON SCL3 tunnel.

It is very important to reduce microphonics to control the superconducting cavity u radio frequency (RF). The liquid helium pressure of the QWR cryomodule is around 1.28 bars in the superconducting cavity at 4.5 K. The fluctuation of helium pressure decreases by changing the flow rate, supply pressure, return pressure, and cryogenic valve control speed, etc. The low-level radio frequency (LLRF) with the self-excited loop (SEL) mode is used to obtain the performance test of the superconducting cavity in the vertical test. The low-level radio frequency (LLRF) can control the cavity with the generator-driven resonator (GDR) controller mode for the beam experiment. The loaded Q, $Q_L$, of the QWR cavity is around $5 \times 10^5$, the $Q_{ext}$ of the pickup is around $1 \times 10^{11}$, the bandwidth of the QWR cavity is about 150 Hz, the pressure sensitivity showing resonance frequency change against helium bath pressure is around 5 Hz/mbar, and Lorentz force detuning (LFD) is around $-15$ Hz/(MV/m)$^2$. The quality factor requirement for the QWR cavity is $2.4 \times 10^8$

at 6.1 MV/m. Variations in helium pressure cause the cavity's resonance frequency to vary in terms of pressure sensitivity; however, they have no effect on the FWHM.

The total heat load for the QWR cryomodule at 6.1 MV/m is around 12 W, in which the static heat load is about 4.5 W. The tuner is used to control the resonance frequency of the cavity and changes the frequency to 81.25 MHz. The tuner is only used to change the frequency when the frequency is off by more than 10 Hz from the resonance frequency of 81.25 MHz. For the first time, the amplitude and phase of the cavity are controlled for one minute. Later, the amplitude and phase of the cavity are controlled for one hour by reducing the fluctuation of the liquid helium pressure under 5 mbar in 20 s. The helium pressure fluctuation is reduced from 20 mbar to 5 mbar in 20 s. The superconducting cavities have different pressure sensitivities; therefore, the cavities respond differently to the helium pressure fluctuation. The amplitude and phase of the cavity can be stabilized as the helium pressure fluctuation decreases. The amplitude fluctuation is less than 1%, and the phase fluctuation is also less than 1 degree for more than an hour for beam commissioning.

Figure 10 shows the pictures of the quarter-wave resonator (QWR) cryomodules and RAON SCL3 tunnel. For the first beam commissioning, the QWR cryomodules from 1 to 6 are used, and the beam energy of $Ar^{9+}$ is increased from 0.5 to 0.7 MeV/u with 30 μA. The second beam commissioning is performed for all QWR cryomodules from 1 to 22 in RAON SCL3, in which the energy of $Ar^{9+}$ is increased from 0.5 to 2.45 MeV/u with 30 μA. The two QWR cryomodules (CMs) for 3 and 20 are excluded because the QWR CM 3 shows the unstable RF control and the QWR CM 20 shows the off-resonance frequency even if the tuner is used at maximum range. The beam energy is determined using the time of flight measurement. For each QWR cavity in the QWR cryomodule, the accelerating amplitude and phase are determined one by one during beam commissioning. The accelerating field and phase for each cavity are kept during beam commissioning.

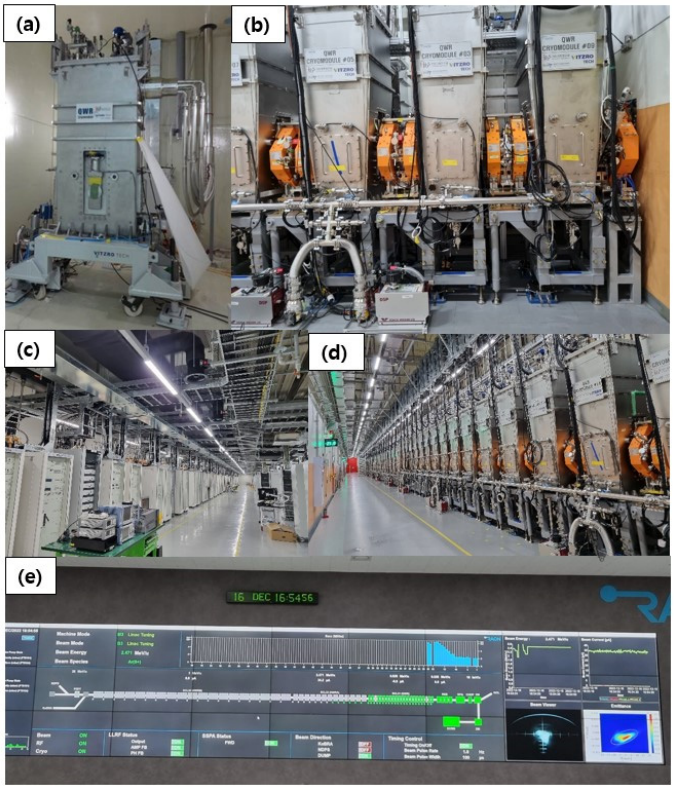



**Figure 10.** Pictures of quarter-wave resonator (QWR) cryomodules: (**a**) the QWR cryomodule in the horizontal test bunker, (**b**) the installed QWR cryomodules on the front side, (**c**) the solid state power amplifier (SSPA) for cryomodules, (**d**) the RAON SCL3 tunnel, and (**e**) the main control screen during beam commissioning.

This research can be useful for the fabrication and testing of superconducting cavities and for understanding the magnetic degradation of the superconducting cavities.

## 7. Conclusions

We have measured the Q slopes for the quarter-wave resonator (QWR) cavities and have shown the magnetic heating effect for the Q factor degradation. The BCS resistance is calculated as a function of temperature for different frequencies in the zero-temperature limit. Magnetic shielding is applied in the cryostat to reduce the magnetic heating of the superconducting cavity coming from an external magnetic field, such as the earth's magnetic field. The magnetic field is reduced below 6 mG in the cryostat by installing both Mu-metal and cryophy. The manufacturing processes for the QWR cavity are shown, and the vertical test is performed for the QWR cavities. The parameters for the QWR cavities are presented. The Q slopes of the QWR cavities are measured with increasing accelerating fields. The Q slope data are changed to the surface resistance so that the surface resistance is expressed according to the peak magnetic field. Magnetic heating causes the degradation of quality factors in the superconducting cavities. From the magnetic degradation, we can find the magnetic moments for the QWR cavities. The medium magnetic moment is obtained as $3.3 \times 10^{-21}$ J/T. The Q slope degradation of the QWR cavities is reasonably explained by the magnetic defects having magnetic moments. All quarter-wave resonator (QWR) cryomodules are installed in the tunnel, and beam commissioning is successfully performed, during which the energy of $Ar^{9+}$ is increased from 0.5 to 2.45 MeV/u. This research shows the Q factor degradation of the QWR cavities using magnetic heating with a magnetic moment. All the discussed processes, which include fabrication, experimentation, and beam commissioning, are shown for the superconducting QWR cavities in this paper.

**Author Contributions:** H.K.: Conceptualization, data curation, investigation, writing—original draft, writing—review and editing., S.J.; data curation, investigation, validation., Y.J.; investigation, validation., J.K.: investigation, validation. All authors have read and agreed to the published version of the manuscript.

**Funding:** This research was supported by the Rare Isotope Science Project (RISP) of the Institute for Basic Science (IBS), funded by the Ministry of Science and ICT and National Research Foundation of Republic of Korea (2013M7A1A1075764).

**Data Availability Statement:** Data is available on request.

**Acknowledgments:** The authors would like to thank all the researchers who contributed to the cavity simulation, cavity fabrication, cavity processes, low-temperature technical support, and beam commissioning experiments in RAON.

**Conflicts of Interest:** The authors declare no conflict of interest.

## References

1. Kim, H.; Jung, Y.; Shin, J.; Kim, S.; Kim, W.K.; Park, G.T.; Lee, S.; Jo, Y.W.; Nam, S.; Jeon, D. RAON superconducting radio frequency test facility construction. In Proceedings of the Linac 2014, Geneva, Switzerland, 31 August–5 September 2014; TUPP086; p. 625.
2. Zhou, D.; Quan, S.; Hao, J.; Lin, L.; Feng, L.; Wang, F.; Zhu, F.; Xie, H.; Zhuang, D.; Cheng, W.; et al. Vertical test system for superconducting RF cavities at Peking University. In Proceedings of the 18th International Conference on RF Superconductivity SRF2017, Lanzhou, China, 17–21 July 2017; TUPB099. JACoW Publishing: Geneva, Switzerland, 2017; p. 631.
3. Reschke, D.; Gubarev, V.; Schaffran, J.; Steder, L.; Walker, N.; Wenskat, M.; Monaco, L. Performance in the vertical test of the 832 nine cell 1.3 GHz cavities for the European X-ray Free Electron Laser. *Phys. Rev. Accel. Beams* **2017**, *20*, 042004. [CrossRef]
4. Ge, R.; Sun, L.; Xu, M.; Ye, R.; Zhang, X.; Sang, M.; Han, R.; Zhang, Z.; Zhang, J.; Bian, L.; et al. 2 K superfluid helium cryogenic vertical test system for superconducting cavity of ADS Injector I. *Radiat. Detect. Technol. Methods* **2020**, *4*, 131. [CrossRef]
5. Fowler, R.H.; Nordheim, L.W. Electron emission in intense electric fields. *Proc. Roy. Soc. A* **1928**, *119*, 173.
6. Gomer, R. *Field Emission and Field Ionization*; Harvard University Press: Boston, MA, USA, 1961.
7. de Heer, W.A.; Chatelain, A.; Ugarte, D. A Carbon Nanotube Field-Emission Electron Source. *Science* **1995**, *290*, 1179. [CrossRef]
8. Richardson, O.W. On the Negative Radiation from Hot Platinum. *Proc. Camb. Philos. Soc.* **1901**, *11*, 286.
9. Wei, X.; Chen, Q.; Peng, L. Electron emission from a two-dimensional crystal with atomic thickness. *AIP Adv.* **2013**, *3*, 042130. [CrossRef]

10. Ang, Y.S.; Yang, H.Y.; Ang, L.K. Universal Scaling Laws in Schottky Heterostructures Based on Two-Dimensional Materials. *Phys. Rev. Lett.* **2018**, *121*, 056802. [CrossRef]
11. Kim, H.; Lee, J.K.; Park, C.-S. Generalized n-dimensional field emission. *J. Korean Phys. Soc.* **2021**, *79*, 363. [CrossRef]
12. Kim, H.; Lee, S. Unified theory of thermionic and field emission for two-dimensional conducting materials. *J. Korean Phys. Soc.* **2022**, *80*, 167. [CrossRef]
13. Sakai, H.; Cenni, E.; Enami, K.; Furuya, T.; Sawamura, M.; Shinoe, K.; Umemori, K. Field emission studies in vertical test and during cryomodule operation using precise x-ray mapping system. *Phys. Rev. Accel. Beams* **2019**, *22*, 022002. [CrossRef]
14. Léger, A. Field emission from a superconductor. *J. Phys. Fr.* **1968**, *29*, 646. [CrossRef]
15. Tan, J. Field emission studies at saclay and orsay. *Part. Accel.* **1996**, *53*, 1.
16. Shu, Q.S.; Gendreau, K.; Hartung, W.; Kirchgessner, J.; Moffat, D.; Noer, R.; Padamsee, H.; Rubin, D.L. Influence of condensed gases on field emission and the performance of superconducting RF cavities. *J. Sears. IEEE Trans.* **1989**, *25*, 1868. [CrossRef]
17. Graber, J.; Crawford, C.; Kirchgessner, J.; Padamsee, H.; Rubin, D.; Sctimueser, P. Reduction of field emission in superconducting cavities with high power pulsed RF. *Nucl. Instrum. Methods Phys. Res. A Accel. Spectrom. Detect. Assoc. Equip.* **1994**, *350*, 572. [CrossRef]
18. Jeon, D.; Hong, I.S.; Kim, H.J.; Kim, J.W.; Bodenstein, R.M.; Cha, H.J.; Choi, S.J.; Choi, O.R.; Do, H.; Choi, B.H.; et al. Design of the RAON accelerator systems. *J. Korean Phys. Soc.* **2014**, *65*, 1010. [CrossRef]
19. Park, G.T.; Kim, W.K.; Jung, Y.; Cha, H.J.; Kim, H. Fabrication of the Prototype β = 0.12 Half Wave Resonator at Rare Isotope Science Project (RISP). *J. Korean Phys. Soc.* **2015**, *67*, 1293. [CrossRef]
20. Kim, W.K.; Kim, H.; Kim, H.J.; Kim, Y.; Lee, M.K.; Park, G.T. Design and Assembly of QWR and HWR Cryomodules, Special Issue on the 18th International Conference on Accelerators and Beam Utilizations. *J. Korean Phys. Soc.* **2015**, *67*, 1287. [CrossRef]
21. Kim, H.; Kim, Y.; Lee, M.; Park, G.T.; Kim, W. Low Temperature Test of HWR Cryomodule. *Appl. Sci. Converg. Technol.* **2016**, *25*, 47. [CrossRef]
22. Jeon, S.; Kim, H.; Jung, Y.; Kim, J.; Lee, J.; Kim, M.; Kim, H.I.; Lee, M. Field emission and x-ray effect on RAON HWR superconducting cavity performance. *Curr. Appl. Phys.* **2022**, *38*, 67. [CrossRef]
23. Zhang, P.; Zhang, X.; Li, Z.; Dai, J.; Guo, L.; Lin, H.; Ma, Q.; Huang, T.; Mi, Z.; Wang, Q.; et al. Development and vertical tests of a 166.6 MHz proof-of-principle superconducting quarter-wave beta = 1 cavity. *Rev. Sci. Instruments* **2019**, *90*, 084705. [CrossRef]
24. Vines, J.; Xie, Y.; Padamsee, H. Systematic Trends for the Medium Field Q-Slope. In Proceedings of the SRF2007, Peking Univ., Beijing, China, 14–19 October 2007; TUP27. p. 178.
25. Weingarten, W.; Eichhorn, R. Field-dependent surface resistance for superconducting niobium accelerating cavities: The case of N doping. In Proceedings of the 17th International Conference on RF Superconductivity (SRF2015), Whistler, BC, Canada, 13–18 September 2015; MOPB010; p. 95.
26. Kim, H.; Jeon, S.; Jung, Y.; Kim, J.; Kim, H. Understanding Q slope of superconducting cavity with magnetic defect and field emission. In Proceedings of the Linac 2022, Liverpool, UK, 28 August–2 September 2022; MOPOGE24. p. 208.
27. Sha, P.; Pan, W.; Zhai, J.; Mi, Z.; Jin, S.; Liu, B.; Dong, C.; He, F.; Ye, L.; He, X.; et al. Quality Factor Enhancement of 650 MHz Superconducting Radio-Frequency Cavity for CEPC. *Appl. Sci.* **2022**, *12*, 546. [CrossRef]
28. Jin, S.; Sha, P.; Pan, W.; Zhai, J.; Mi, Z.; He, F.; Dong, C.; Ye, L.; He, X. Development and Vertical Tests of CEPC 650-MHz Single-Cell Cavities with High Gradient. *Materials* **2021**, *14*, 7654. [CrossRef] [PubMed]
29. Kutsaev, S.V.; Taletski, K.; Agustsson, R.; Carriere, P.; Cleland, A.N.; Conway, Z.A.; Dumur, É.; Moro, A.; Smirnov, A.Y. Niobium quarter-wave resonator with the optimized shape for quantum information system. *EPJ Quantum Technol.* **2020**, *7*, 7. [CrossRef]
30. Park, S.H.; An, J.; Bang, J.; Hahn, S. Simulation of superconducting cavities for quantum computing. *Prog. Supercond. Cryog.* **2019**, *21*, 22.
31. Padamsee, H.S. Superconducting Radio-Frequency Cavities. *Annu. Rev. Nucl. Part.* **2014**, *64*, 175. [CrossRef]
32. Byers, N.; Yang, C.N. Theoretical considerations concerning quantized magnetic flux in superconducting cylinders. *Phys. Rev. Lett.* **1961**, *7*, 46. [CrossRef]
33. Okada, T.; Kako, E.; Masuzawa, M.; Sakai, H.; Ueki, R.; Umemori, K.; Tajima, T. Observation of quenching-induced magnetic flux trapping using a magnetic field and temperature mapping system. *Phys. Rev. Accel. Beams.* **2022**, *25*, 082002. [CrossRef]
34. Saito, K. Q slope analysis of Niobium SC RF cavities. In Proceedings of the 11th Workshop on RF Superconductivity, Lübeck, Germany, 8–12 September 2003; ThP17; p. 643.
35. Miyazaki, A.; Delsolaro, W.V. Two different origins of the Q-slope problem in superconducting niobium film cavities for a heavy ion accelerator at CERN. *Phys. Rev. Accel. Beams* **2019**, *22*, 073101. [CrossRef]
36. Kim, H.; Jung, Y.; Choi, J.W.; Jo, Y.W.; Lee, M.; Kim, M.S.; Kim, J.; Kim, Y.; Jung, H. Temperature measurement of cryomodules. In *HB2018, Proceedings of the 61st ICFA Advanced Beam Dynamics Workshop on High-Intensity and High-Brightness Hadron Beam, Daejeon, Korea, 17–21 June 2018*; WEP2PO016; JACoW Publishing: Geneva, Switzerland, 2018; p. 299.
37. Kim, H.; Chang, Y.S.; Kim, W.K.; Jo, Y.W.; Kim, H.J. Introduction to helium leak detection techniques for cryogenic systems. *Appl. Sci. Converg. Technol.* **2015**, *24*, 77. [CrossRef]
38. Ginsburg, C.M.; Reid, C.; Sergatskov, D.A. Magnetic shielding for the Fermilab vertical cavity test facility. *IEEE Trans. Appl. Supercond.* **2009**, *19*, 1419. [CrossRef]
39. Sankar, M.; Mirji, K.V.; Prasad, V.V.S.; Baligidad, R.G.; Gokhale, A.A. Purification of niobium by electron beam melting. *High Mater. Proc.* **2016**, *35*, 621. [CrossRef]

40. Casalbuonia, S.; Knabbeb, E.A.; Kotzlera, J.; Liljeb, L.; Sawilskia, L.; Schmuserc, P.; Steffenb, B. Surface superconductivity in niobium for superconducting RF cavities. *Nucl. Instrum. Methods Phys. Res. A Accel. Spectrom. Detect. Assoc. Equip.* **2005**, *538*, 45. [CrossRef]
41. Zhang, P.; Lau, Y.Y.; Gilgenbach, R.M. Analysis of radio-frequency absorption and electric and magnetic field enhancements due to surface roughness. *J. Appl. Phys.* **2009**, *105*, 114908. [CrossRef]
42. Sara, H. An Analytical Approach for Calculating the Quench Field in Superconducting Cavities. In Proceedings of the 1995 Workshop on RF Superconductivity, Gif-sur-Yvette, France, 17–20 October 1995; SRF95C10. p. 413.
43. Safa, H. Statistical analysis of the quench fields in scrf cavities. In Proceedings of the 1997 Workshop on RF Superconductivity, Padova, Italy, 6–10 October 1997; SRF97C11; p. 503.
44. Padamsee, H.; Knobloch, J.; Hays, T. *RF Superconductivity for Accelerators*; Wiley-VCH Verlag GmbH&Co. KGaA: Hoboken, NJ, USA, 2008.
45. Jung, Y.; Kim, H.; Kim, W.K.; Lee, J.; Seo, J. Status of RRR analysis for RAON accelerator. In Proceedings of the LINAC2016, East Lansing, MI, USA, 25–30 September 2016; TUP106004; p. 594.


**Disclaimer/Publisher's Note:** The statements, opinions and data contained in all publications are solely those of the individual author(s) and contributor(s) and not of MDPI and/or the editor(s). MDPI and/or the editor(s) disclaim responsibility for any injury to people or property resulting from any ideas, methods, instructions or products referred to in the content.